ELSEVIER

Solar Energy Materials & Solar Cells 71 (2002) 295–312

Solar Energy Materials & Solar Cells

www.elsevier.com/locate/solmat

A contactless photoconductance technique to evaluate the quantum efficiency of solar cell emitters

Andrés Cuevas*, Ronald A. Sinton[1], Mark Kerr, Daniel Macdonald, Helmut Mäckel

Faculty of Engineering and Information Technology, Centre for Sustainable Energy Systems, Australian National University, Canberra ACT 0200, Australia

Received 20 November 2000; received in revised form 23 May 2001; accepted 18 June 2001

Abstract

A new technique, the spectral response of the steady-state photoconductance, is proposed for solar cell characterisation in research and development. The emphasis of this paper is on the evaluation of the carrier collection efficiency of the emitter region based on a simple, two-wavelength approach. We show that in addition to the well-established determination of the wafer recombination properties that results from a long-wavelength photoconductance measurement, detailed emitter quantum-efficiency information can be obtained by performing a second measurement with short-wavelength light. The method is experimentally demonstrated with silicon solar cell precursors having emitters with markedly different levels of surface and bulk recombination losses. The main advantages of the spectral photoconductance technique are that it is fast, contactless, and can be used immediately after junction formation before metallisation; these properties make it very appropriate for routine monitoring of the emitter region, including in-line process control.

Keywords: Photoconductance; Quantum efficiency; Spectral response; Lifetime; Solar cells

1. Introduction

The spectral response of a solar cell, that is, the short-circuit current per unit incident illumination power as a function of wavelength, is commonly used to

*Corresponding author. Tel.: +61-26-1253702; fax: +61-2-6125-0506.
E-mail address: andres.cuevas@anu.edu.au (A. Cuevas).
[1] Sinton Consulting, Inc., 1132 Green Circle, Boulder, CO 80305, USA.

0927-0248/02/$ - see front matter
PII: S0927-0248(01)00089-7

investigate its ability to collect carriers generated by the different wavelengths of light that compose the solar spectrum. It is particularly useful to characterise the emitter, whose dopant density profile must be carefully optimised in order to fit in the narrow compromise between designs for high short-circuit current and for low series resistance. Despite their usefulness, spectral response measurements are hindered by the fact that they require finished devices and a relatively complex experimental set-up. This paper explores the extent to which similar information to the traditional spectral response can be obtained using simpler, contactless spectral photoconductance measurements.

Photoconductance measurements are increasingly being used to characterise various aspects of silicon wafers and solar cells. The photoconductance is a measure of the effective lifetime of minority carriers in the wafer. Generally, this effective lifetime is interpreted to obtain information about different recombination mechanisms. The introduction of the quasi-steady-state technique (briefly, QSSPC) [1] has expanded the range of possible applications [2,3] and facilitated detailed studies of the injection-level dependence of carrier recombination [4]. Certain variants of the measurement conditions give an enhanced sensitivity to specific physical mechanisms [5], which is useful for device diagnosis. For example, recent work has addressed the separation between bulk and surface recombination by comparing transient and steady-state measurements [6], or by comparing short-wavelength to long-wavelength measurements [7].

The fact that photoconductance based measurements of carrier lifetimes are not, in general, impervious to the spectral content of the illumination can be, and frequently is, ignored. There are, however, cases where such a simplified view can lead to erroneous results. The case of a silicon wafer with a heavily doped region, or emitter, on the front surface (lifetime test structures usually have a second, symmetrical emitter on the rear surface) deserves attention because it represents the prevalent solar cell structure. Previous photoconductance based studies of emitter regions [8] used white light similar to the solar spectrum and neglected the fact that a significant fraction of it can be absorbed within the emitter region itself. For example, a 1-μm-thick emitter absorbs nearly 30% of the standard AM1.5G spectrum. Depending on the specific features of the emitter, in particular, its dopant concentration and surface recombination velocity, many carriers generated within it may recombine rapidly in place before they can contribute to the photoconductance of the wafer. In other words, from the point of view of the photoconductance, the amount of usable photogeneration can be significantly reduced by emitter losses. For example, a high emitter recombination can produce a 15% photocurrent loss in a 1-μm-thick emitter. For accurate QSSPC lifetime measurements this source of error can be suppressed by filtering out the shorter wavelengths (less than 600 nm) of the white light. This precaution is especially important if very highly doped, non-passivated and deep diffusions are present.

What, if ignored, is a source of error, can be converted into a useful characterisation tool. Emitter losses can be exacerbated by using short-wavelength illumination, which is almost completely absorbed within the emitter. This makes the steady-state photoconductance of a wafer strongly dependent on the emitter

quantum collection efficiency. On the other hand, the latter has very little impact on the photoconductance for longer wavelength light, and this provides a basis for comparison. This means that the wafer photoconductance can be used as the detector of emitter quantum efficiency. The calibration factor for this detector is the effective lifetime of the wafer, which can be measured with longer wavelength light. This paper proposes and demonstrates the use of spectral photoconductance measurements just after junction formation to characterise solar cell emitters.

2. Spectral response of the photoconductance: computer simulations

When a wafer is illuminated, the electron and hole densities increase over their equilibrium values and this produces an augmented conductivity of the material. The excess photoconductance, $\Delta\sigma_L$, is obtained by integrating over the wafer thickness, W, the excess carrier concentration, Δn, multiplied by the carrier mobilities and the electronic charge:

$$\Delta\sigma_L = q\int_0^W (\mu_n + \mu_p)\Delta n \, dx. \tag{1}$$

To simulate the dependence of the photoconductance with the wavelength of the illumination we have used the computer program PC1D [9]. In this program, the function that gives the excess photoconductance is called *cumulative excess conductivity*. The simulation of the photoconductance is performed in open-circuit, which is representative of the zero current conditions typical of our contactless experimental measurements. By changing the simulation conditions to short-circuit, the program can also be used to calculate the traditional spectral response and quantum efficiency curves of the device.

To provide a context for the experimental technique described in the following, we have compared the traditional spectral response of the short-circuit current to the response of the open-circuit photoconductance in three different cases. Fig. 1 shows a case where the shapes of these two curves are identical. The parameters used for the computer modelling were: wafer thickness 300 μm, p-type, resistivity 1 Ω cm, carrier lifetime 1000 μs, front and rear surface recombination velocities of 10^3 and 10 cm/s, respectively, Gaussian n-type emitter of 100 Ω/sq, surface concentration of $3\times10^{19}\,\mathrm{cm}^{-3}$ and junction depth 0.6 μm. The surface was assumed to be planar and coated with a 70-nm-thick antireflection layer with refractive index 2.1. The back and front internal reflectance was assumed to be 70%. These lifetime and surface recombination velocity values are representative of the best material parameters measured in the highest quality silicon solar cells. The calculated output parameters of this device at standard illumination (0.1 W/cm^2, AM1.5G spectrum) and temperature (25°C) conditions are $J_{sc} = 37.5\,\mathrm{mA/cm^2}$, $V_{oc} = 700\,\mathrm{mV}$, $\eta = 22\%$. The total excess photoconductance at open-circuit corresponding to this illumination is $\Delta\sigma(\mathrm{AM1.5G}) = 19.6\,\mathrm{mS}$. As described in detail in [5], there is a direct correlation between photoconductance and open-circuit voltage. As this example illustrates, a

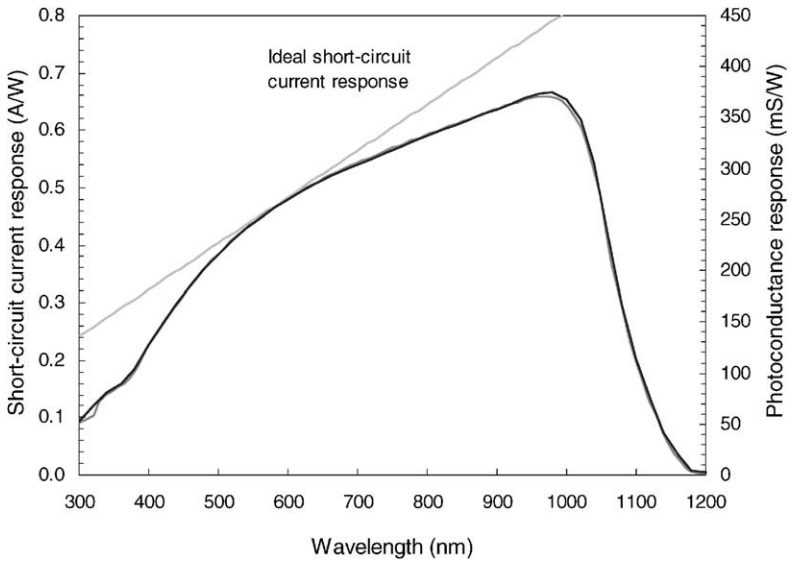

Fig. 1. Modelled spectral photoconductance and short-circuit current as a function of wavelength. The curve shapes are identical for this high-efficiency silicon solar cell structure having a passivated emitter surface ($S_{\text{front}} = 10^3$ cm/s). The straight line is the ideal limit of the short-circuit current response.

high photoconductance, such as 19.6 mS, is representative of a high performance device.

Fig. 2 shows the modelled spectral responses for case II, which is the same high-efficiency solar cell modelled in Fig. 1, except that the front surface recombination velocity was increased from 1000 to 2×10^5 cm/s. Simulations indicate that this has two main effects on the solar cell. First, the de-passivation of the front surface causes an open-circuit voltage loss from 700 down to 635 mV. Second, there is a loss of 60% of current response at 400 nm. The remaining one-sun characteristics are $J_{\text{sc}} = 35.7\,\text{mA/cm}^2$, $\eta = 19\%$, $\Delta\sigma(\text{AM1.5G}) = 1.9\,\text{mS}$. The traditional spectral response curve and the photoconductance response curve agree well in the 400–800 nm range, then diverge in the IR. The divergence in the IR is due to very high front saturation current density, J_{oe}, on the de-passivated emitter. Photogeneration deep in the wafer results in higher steady-state photoconductance than photogeneration near the front of the wafer [7]. What happens is that the high-recombination at the front surface can become diffusion limited for photogeneration deep into the wafer. This enhanced IR response is a trend not seen in the spectral response of the short-circuit current. Notice that a photoconductance measurement at 700 or 800 nm would have detected an effective lifetime drop by a factor of 10 (see the different scale of the secondary ordinate in Figs. 1 and 2), and predicted a 60 mV loss of V_{oc}. By using an additional short-wavelength measurement, the loss of short-circuit current in the blue due to the emitter may be detected as well.

The difference between the curves of the spectral response of the short-circuit current and the ideal limit is a measure of several fundamental properties of the solar

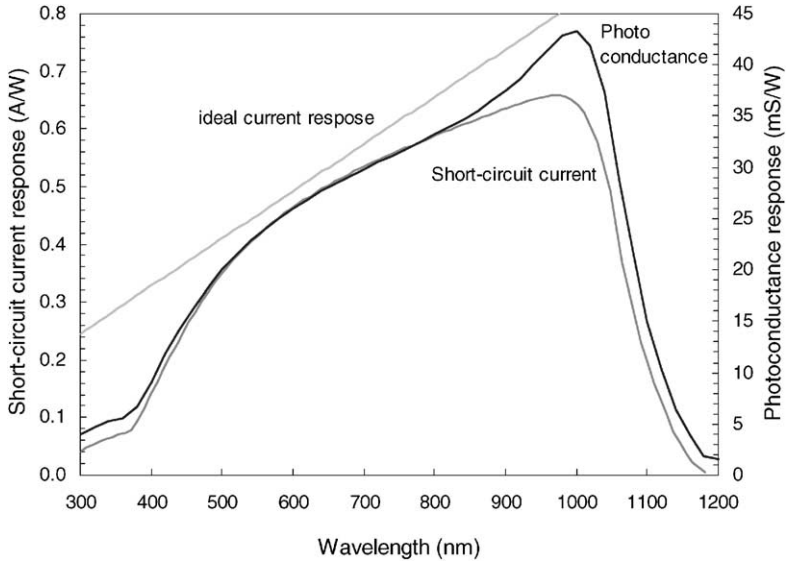

Fig. 2. PC1D simulations for the same case as in Fig. 1, but with a surface recombination velocity of $S_{\text{front}} = 2 \times 10^5$ cm/s.

cell. Optical reflection losses and incomplete IR light absorption give an upper bound to the spectral response curve. This upper bound is practically reached in the case of Fig. 1, where electronic losses are minimal. Further losses in the UV indicate emitter quantum efficiency less than one. As mentioned before, the photoconductance measures these losses because only a fraction of the carriers generated within the emitter layer survive the strong recombination usually produced by the heavy dopant density and by the surface and are able to eventually contribute to the photoconductance. Additional losses in the IR, such as those happening in the third example shown in Fig. 3, are indicative of low diffusion length and poor back surface passivation.

Fig. 3 shows a simulation relevant to an industrial silicon solar cell where significant recombination losses occur at both short and long wavelengths. For this case III simulation, we have used an emitter dopant profile typical of a supersaturated phosphorus diffusion, with a surface concentration of 3×10^{20} 1/cm^3 and a 0.04 μm dead layer, sheet resistance of 50 Ω/sq, and junction depth of 0.4 μm. The carrier lifetime in the base has now been assumed to be 10 μs, the front surface recombination velocity 3×10^6 cm/s, and the effective surface recombination velocity at the rear 10^3 cm/s, a value representative of an aluminium alloyed p^+ region. The optical parameters, wafer thickness and resistivity were the same as used in the previous case. The calculated output parameters of this device at standard conditions are $J_{sc} = 32.3$ mA/cm^2, $V_{oc} = 610$ mV, $\eta = 16.2\%$ (no shading or resistive losses). The total excess photoconductance is $\Delta\sigma(\text{AM1.5G}) = 0.21$ mS. Comparing the three cases, it is clear that the absolute magnitude of the photoconductance varies

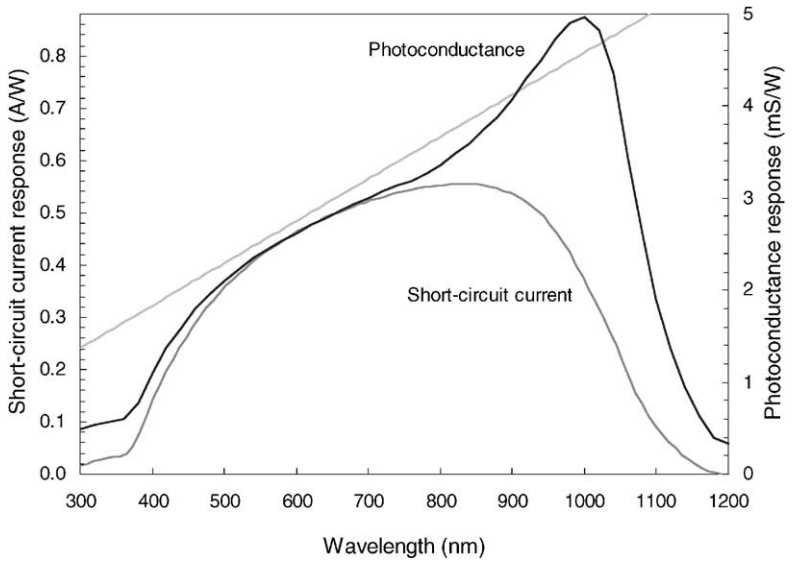

Fig. 3. Spectral photoconductance response and short-circuit current response modelled for the case of a commercial silicon solar cell. Poor current response in the UV and IR are due to emitter and base region losses, respectively. Note that the photoconductance response also shows the UV loss, but not the IR loss.

greatly with the global recombination properties of the wafer. The calculation of the effective minority carrier lifetime from the photoconductance is described in [1] and, in a condensed manner, in Section 4. The effective lifetimes for the three different wafers considered above are 356, 35 and 3.8 μs for cases I, II and II, respectively.

The short-circuit current response of the industrial solar cell is considerably reduced both in the violet and IR regions of the spectrum. The photoconductance response is greater than the short-circuit current response in these UV and IR regions, relative to their respective responses at $\lambda = 700$ nm. The photoconductance response shows a maximum at $\lambda = 1000$ nm, despite the obvious degradation of the short-circuit current response due to the relatively short diffusion length (164 μm). The reason for this different behaviour is that carriers generated deep in the wafer still contribute to the excess conductance even if they cannot reach the pn junction. Additionally, the effective lifetime for deep photogeneration is higher [7], as in the second example. The discrepancy at short wavelengths is due to the fact that there is a contribution of the emitter region to the excess photoconductance for UV light, while such contribution is essentially zero in the case of the short-circuit current. The emitter contribution to the photoconductance (including one half of the space charge region) at $\lambda = 410$ nm is approximately 18% for this particular device (case III). This contribution is negligible for cases I and II because the long base lifetimes and rear surface passivation lead to a buildup of carrier density in the base that dwarfs the emitter contribution to photoconductance. It is interesting to note that although the short-circuit current response in the UV can be very close to zero, the

photoconductance response is unlikely to reach this limit since the photoconductance in the emitter will be sensed even if the carriers cannot reach the junction and the base. This leads to a divergence between the curves in the case where the emitter spectral current response approaches zero, yet the photoconductance goes to a low, non-zero value.

3. A practical two-wavelength method

Although it is possible to measure complete spectral response curves, we will focus here on a simple approach to monitor quantum collection losses in the emitter based on measuring the photoconductance at two, properly selected wavelengths of light. As indicated by the modelling in the previous section, a wavelength in the vicinity of 400 nm is suitable to sense the properties of the emitter. In the traditional short-circuit current approach, a single measurement at a violet or UV wavelength would suffice, since the spectral response can be automatically normalised to its maximum possible value, given by $SR_{ideal} = \lambda(\mu m)/1.2398$, where λ is the wavelength of illumination expressed in μm and the factor 1.2398 is the wavelength in vacuum of a 1 eV photon, that is, hc/q, with h being Plank's constant, c the velocity of light in vacuum and q the electron's charge. The normalised spectral response is called the external quantum efficiency, EQE, a meaningful concept that gives the fraction of incident photons that are converted into output electrons. The EQE is given by the ratio of the short-circuit current density to the incident photon flux on the surface of the solar cell, N_{ph}:

$$EQE \equiv \frac{J_{sc}(\lambda)}{qN_{ph}(\lambda)}. \tag{2}$$

The photon flux can be obtained from the incident power density (in W/cm^2) and the wavelength of illumination (in μm):

$$N_{ph}(\lambda) = P_{in}(\lambda)\frac{\lambda}{hc} = P_{in}(\lambda)\, 5.034 \times 10^{18}. \tag{3}$$

A single wavelength measurement of the absolute value of the spectral response is prone to be more uncertain than a multi-wavelength measurement. A more robust approach to a simple spectral characterisation would be to include a second measurement at a reference wavelength and determine the relative spectral response:

$$EQE(J_{sc})|_{relative} \equiv \frac{J_{sc}(\lambda)}{J_{sc}(\lambda_{ref})}\frac{P_{in}(\lambda_{ref})}{P_{in}(\lambda)}\frac{\lambda_{ref}}{\lambda}. \tag{4}$$

In a similar way, we can determine the ratio between two photoconductance values measured at different wavelengths of light:

$$EQE(\Delta\sigma_L)|_{relative} \equiv \frac{\sigma(\lambda)}{\sigma(\lambda_{ref})}\frac{N_{ph}(\lambda_{ref})}{N_{ph}(\lambda)}, \tag{5}$$

where we have converted the incident illumination power P_{in} to a photon flux N_{ph}, using Eq. (3). Eq. (5) constitutes the definition of a photoconductance-based external

quantum efficiency, EQE($\Delta\sigma_L$). It should be emphasised that the similarity between Eqs. (4) and (5) does not imply that EQE($\Delta\sigma_L$) is identical to the traditional EQE(J_{sc}). On the contrary, the physical mechanisms that are prevalent in open-circuit and short-circuit conditions can be different, leading to possible differences between these two external quantum efficiencies. Both are, nevertheless, closely related, and as meaningful physical information can be obtained from EQE($\Delta\sigma_L$) as from EQE(J_{sc}).

In practice, it is important to realise that the photoconductance can vary in a non-linear fashion with the incident light power. This is due to the fact that the effective lifetime generally depends on the excess carrier density at which it is measured, as different recombination mechanisms come into effect. It is, therefore, important to perform the UV and IR measurements so that both result in the same excess carrier density within the wafer. A practical way to achieve this is to log the ratio of incident photon flux required to give the same photoconductance at the two wavelengths, that is

$$\mathrm{EQE}(\Delta\sigma_L)|_{\mathrm{relative}} \equiv \left.\frac{N_{\mathrm{ph}}(\lambda_{\mathrm{ref}})}{N_{\mathrm{ph}}(\lambda)}\right|_{\sigma=\mathrm{constant}}. \tag{6}$$

The selection of an appropriate reference wavelength is important for the method to be meaningful. From the three examples given in Section 2, it appears that the choice of specific UV and IR wavelengths may need to be slightly different in every case. As shown in Fig. 1, photoconductance is equivalent to spectral response for high-efficiency solar cell structures. These wafers have long diffusion lengths and good front and rear surface passivation. In this special case, any reference wavelength in the 700–1000 nm range will work equally well, with longer wavelengths being slightly preferable in order to minimise the photogeneration within the emitter. In a more common device with a short diffusion length, high back-surface recombination, or high emitter J_o, such as case III, a medium wavelength producing generation primarily in the front part of the wafer is a better choice, since it will give a very similar carrier density profile and effective lifetime as the short-wavelength light. For example, a wavelength of 700 nm has an absorption depth of 5.3 μm. This will still give generation primarily in the base region for typical emitters. In the spatial scale of the wafer thickness (typically 300 μm), the photogeneration will be similar to the short-wavelength light in terms of the resulting carrier distribution that determines the effective lifetime. The analysis in Eq. (6) would be adequate for monitoring the loss of emitter response shown in Fig. 2, as long as the IR wavelength for comparison was less than 800 nm. Looking at Fig. 3, a good monitor for the emitter quantum efficiency for an industrial cell would be to track the ratio of photoconductance response at 400 nm vs. 700 nm. This ratio would also be a good indicator of the traditional spectral response of the short-circuit current at these wavelengths.

To illustrate the method, we have applied it to the three cases discussed in Section 1. The simulation of the photoconductance had to be done over a broad range of light intensities, in order to apply Eq. (6) properly, that is, when both the 400 and 700 nm illuminations result in the same excess photoconductance. The results, given

in Table 1, indicate a good agreement between the new method and the traditional one. The relative external quantum efficiencies, given by Eqs. (6) and (4), respectively, differ by 3.5% at the most. The discrepancy is even lower after analysing the external quantum efficiency to determine the internal quantum efficiency IQE, as shown by the third and sixth columns of Table 1. The determination of the internal emitter collection efficiency, $\eta_{\text{c-emitter}}$, is discussed in the next section.

In summary, when the effective lifetime in the base is very long, the measured photoconductance is a precise indication of the traditional spectral response. Combinations of very low effective lifetime in the base, very low emitter collection efficiencies, high emitter J_o, or very thick emitters can, however, compromise the validity of the assumptions and the accuracy of the simple analysis described here. For a particular technology or production process, the precise test conditions should be refined and their region of relevance established. Simulation with PC1D, as in the three examples in Section 2, can be used to optimise the measurement wavelengths that will allow the determination of the desired spectral characteristic. Additional precision would result from monitoring the measured $\eta_{\text{c-emitter}}$ and $\tau_{\text{eff(bulk)}}$. A range of acceptable values for these parameters can be defined that will guarantee a given upper bound on the uncertainty in the analysis.

4. Extraction of the internal emitter collection efficiency

As mentioned above, absolute measurements of the spectral response of the short-circuit current can be converted to quantum collection efficiency. An example is given in Fig. 4. A more profound analysis of the EQE can be done by separating the optical and electronic mechanisms that determine it [10]. The EQE can be expressed as the product of the fraction of incident photons that are absorbed in the sample, f_{abs}, and the probability that the carriers generated by those photons are collected at the junction, η_c:

$$\text{EQE} = f_{\text{abs}}\eta_c. \tag{7}$$

Table 1
Comparison between the new photoconductance-based and the traditional short-circuit current methods for the determination of the short-wavelength quantum collection efficiency[a]

	Photoconductance method		Short-circuit current method		
	$\text{EQE}(\Delta\sigma_L)$	$\text{IQE}(\Delta\sigma_L)$	$\text{EQE}_{\text{relative}}$	$\text{EQE}_{\text{absolute}}$	IQE
Case I	0.7383	1.0035	0.726	0.70	0.989
Case II	0.4659	0.6332	0.462	0.437	0.6184
Case III	0.4562	0.6201	0.472	0.436	0.6166

[a] The results of PC1D simulations are given for three different cases of silicon solar cells. The first columns are values of quantum efficiency at 400 nm relative to those at 700 nm, while the last two columns give the absolute values at $\lambda = 400$ nm given by the standard method.

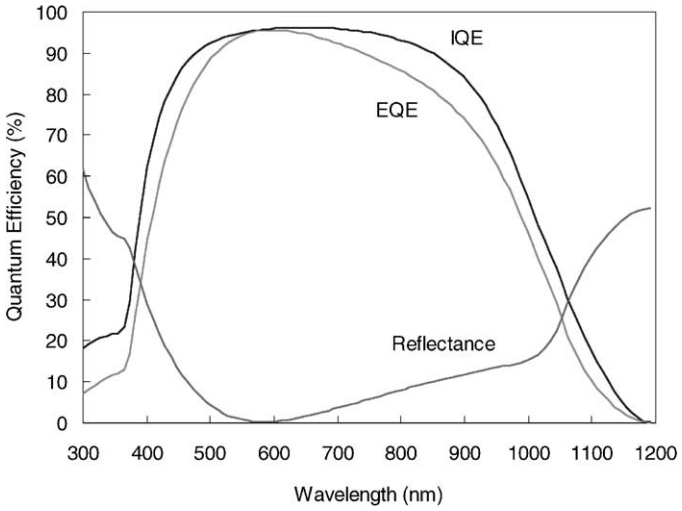

Fig. 4. Internal and external quantum efficiency corresponding to the modelled short-circuit current response of Fig. 3.

The right-hand side of Eq. (7) can be further decomposed to separate the base and emitter contributions:

$$\mathrm{EQE} = f_{\text{abs-base}}\eta_{\text{c-base}} + f_{\text{abs-emitter}}\eta_{\text{c-emitter}}. \tag{8}$$

Eq. (8) describes the classic way in which the quantum efficiency is modelled theoretically, by adding the contributions from the different regions of the solar cell. A third term to account for the photogeneration within the space-charge region is frequently added, but in the case of conventional silicon cells it can be lumped into the base region term with little error.

The overall shape of the EQE curve is affected by the external reflectance at all wavelengths. This imposes an upper bound on the *internal* quantum efficiency, which is defined as

$$\mathrm{IQE} = \frac{\mathrm{EQE}}{1 - R}, \tag{9}$$

where R is the total reflectance. The difference between EQE and IQE is shown graphically in Fig. 4. Note that the IQE is not identical to the carrier collection probability, η_c, although it practically is in the wavelength range up to 950 nm for typical, 300-μm-thick silicon solar cells. In the short wavelength region, below 450 nm, the light is absorbed primarily in the doped front emitter of the solar cell, and the shape of the curve is determined by the competition between carrier collection at the junction and recombination at the surface and in the heavily doped volume of the emitter. For wavelengths beyond 500 nm, the shape of the IQE curve is primarily indicative of recombination in the volume of the base and at the rear surface. For wavelengths exceeding 1000 nm, the absorption is very deep within the

wafer and the curve shape strongly depends on light-trapping and the optical design of the device. The IQE at very long wavelengths is not only a function of the electronic properties of the device and it is generally much lower than the carrier collection probability, η_c.

Spectral photoconductance measurements can also be analysed to extract the underlying physical mechanisms. For simplicity, let us consider a wafer with passivated front and rear surfaces and a bulk diffusion length longer than the wafer thickness. In such a case, the excess carrier density is approximately constant and its average value, Δn_{av}, can be straightforwardly determined from the measured excess photoconductance if the wafer thickness, W, and the carrier mobilities are known

$$\Delta\sigma_L = qW(\mu_n + \mu_p)\Delta n_{av}. \tag{10}$$

The excess carrier density and, therefore, the excess photoconductance is proportional to the photon flux. The relationship between Δn_{av} and N_{ph} can be determined from the balance between the recombination and the photogeneration rates in the wafer:

$$\frac{\Delta n_{av}}{\tau_{eff}} W = f_{abs} N_{ph}, \tag{11}$$

where τ_{eff} is the minority carrier effective lifetime [1]. This steady-state lifetime is proportional to the photoconductance, so the two are largely interchangeable:

$$\Delta\sigma_L = q(\mu_n + \mu_p)\tau_{eff} f_{abs} N_{ph}. \tag{12}$$

In general, the excess carrier density Δn can be non-uniform. The classic solution of the continuity equations in steady-state with the boundary condition of open-circuit may be used to calculate the function $\Delta n(x)$ and show analytically the dependence of the spectral photoconductance on the specific boundary conditions at the front and back surfaces of the wafer. An example of such detailed analysis can be found in [7]. Alternatively, numerical solutions such as those implemented in the program PC1D can be used, as we did in Section 1. Nevertheless, even if the physical situation can be quite complex, it is convenient to simplify it by using an average carrier density, defined by Eq. (10), and an effective lifetime, defined by Eq. (11), because these parameters can be obtained from two easily measurable magnitudes, the photoconductance and the photon flux. This simplified treatment will be maintained here, with some modifications to accommodate emitter effects.

When considering monochromatic illumination with very-short wavelengths, which are absorbed near the front surface, a more detailed evaluation of the sources of measurable photoconductance is required. As indicated by computer modelling, the total cumulative photoconductance is (even for UV illumination) primarily produced in the base region. This is due to its larger volume, higher carrier mobility, and higher minority carrier density due to lower doping. This means that the base-centred approach inherent to the definition of effective lifetime is still applicable to cases where a significant fraction of the light is absorbed in the emitter region. That is, the parameters Δn_{av} and W in Eq. (8) refer to the excess carrier density and thickness of the base region. In this base-centred approach, the *effective*

photogeneration rate that is relevant for the calculation of the effective lifetime, $N_{ph} f_{abs}$, is not always equal to the sum of base and emitter components, $N_{ph}(f_{abs\text{-}base} + f_{abs-emitter})$, but needs to also be referred to the base region. Carriers generated within the emitter will contribute to the photoconductance of the base only after carrier transport through the emitter and a fraction of them will be lost before they can be collected at the pn junction and injected into the base. As a consequence, the photoconductance, given by Eq. (12) can be formally expressed to be a function of the emitter collection efficiency, $\eta_{c\text{-}emitter}$:

$$\Delta\sigma_L = q(\mu_n + \mu_p)\tau_{eff}\, N_{ph}(f_{abs\text{-}base} + f_{abs\text{-}emitter}\eta_{c\text{-}emitter}). \tag{13}$$

This is equivalent to considering the electron-hole pairs injected from the emitter into the lightly doped portion of the wafer as an extra source of photoconductance, in addition to those actually photogenerated within the lightly doped part of the wafer. These "extra" electron-hole pairs must be accounted for in the detailed balance under steady-state conditions.

Consider now the case of illuminating the wafer with short-wavelength light, for example $\lambda = 410\,\text{nm}$, which was used in the experimental work presented in the following section. The corresponding absorption coefficient in silicon is $6.7 \times 10^4\,\text{cm}^{-1}$, which implies that most of this violet light is absorbed within 0.15 μm of the surface, which is smaller than the thickness of typical phosphorus diffusions for silicon solar cells, about 0.4 μm. For light that is absorbed entirely in the emitter, the term of Eq. (13) representing generation within the base, $f_{abs\text{-}base}$, drops out and we have

$$\Delta\sigma_{L(UV)} \approx q(\mu_n + \mu_p)\tau_{eff} N_{ph(UV)} f_{abs(UV)} \eta_{c\text{-}emitter(UV)}. \tag{14}$$

Comparing Eqs. (12) and (14), it can be noticed that the standard lifetime analysis expressed by Eq. (12) would result in an effective lifetime that actually is $\tau_{eff}\eta_{c\text{-}emitter}$ in the special case of UV light, that is, a lifetime that would be underestimated by the factor $\eta_{c\text{-}emitter}$.

Consider next a longer wavelength in the range 700–1000 nm. The generation in the emitter becomes a negligible fraction of the total, the term $f_{abs\text{-}emitter}\eta_{c\text{-}emitter}$ in Eq. (13) drops out and the effective lifetime of the wafer is practically independent of the emitter optical and quantum collection properties in this case

$$\Delta\sigma_{L(IR)} \approx q(\mu_n + \mu_p)\tau_{eff}\, N_{ph(IR)} f_{abs(IR)}. \tag{15}$$

The ratio between two photoconductance measurements at short and long wavelengths as determined by Eqs. (14) and (15), respectively, approximately yields the emitter internal quantum collection efficiency $\eta_{c\text{-}emitter}$ for violet light. As mentioned in Section 3, it is important that the two photon fluxes are adjusted to obtain the same photoconductance, so the effective lifetime is the same in both cases. Dividing Eq. (14) by Eq. (15) with $\Delta\sigma_{L(UV)} = \Delta\sigma_{L(IR)}$ we obtain

$$\eta_{c\text{-}emitter(UV)} \approx \frac{f_{abs(IR)}}{f_{abs(UV)}} \frac{N_{ph(IR)}}{N_{ph(UV)}}\bigg|_{\sigma=\text{constant}}. \tag{16}$$

Comparing this expression to Eq. (6) we observe that the only difference between the external and internal quantum efficiencies is the presence of the optical absorption factors in the latter. This is, of course, similar to the relationship between the internal and external quantum efficiencies obtained from short-circuit current measurements expressed by Eq. (9).

The two approaches to obtain the emitter collection efficiency, from the photoconductance and the short-circuit current, are compared in Table 1. The results of PC1D simulations of the three cases studied in Section 2 indicate excellent agreement between both methods, with the photoconductance resulting in a very small overestimation of the emitter internal quantum efficiency. The absorption fractions corresponding to the simulated devices, which had a single layer antireflection coating, were calculated to be $f_{\mathrm{abs(400\ nm)}} = 0.707$ and $f_{\mathrm{abs(700\ nm)}} = 0.965$, respectively.

Instrumentation that measures photoconductance usually reports lifetime and uses the standard analysis expressed by Eq. (12), even if, as we have discussed, this can lead to an erroneous determination of the lifetime for short-wavelength illumination. If this standard analysis is used, the lifetimes measured with UV and IR illumination will, in general, be different, $\tau_{\mathrm{eff(UV)}} \neq \tau_{\mathrm{eff(IR)}}$. The emitter quantum collection efficiency can then be obtained from the two standard determinations of the lifetime at short and long wavelengths:

$$\eta_{\mathrm{c\text{-}emitter(UV)}} \approx \left.\frac{\tau_{\mathrm{eff(UV)}}}{\tau_{\mathrm{eff(IR)}}}\right|_{\Delta n=\mathrm{constant}}. \tag{17}$$

In the next section we use this latter approach because it follows more closely the common interpretation of steady-state photoconductance measurements.

As Eq. (16) indicates, determination of the internal quantum collection efficiency $\eta_{\mathrm{c\text{-}emitter}}$ of the emitter region requires measurement of the reflection, as well as the photon flux and photoconductance. For rapid, in-line monitoring of emitter regions, the external collection efficiency approach outlined in Section 3 may be preferable.

5. Experimental demonstration

Four p-type FZ silicon wafers were diffused on both sides using a $POCl_3$ source at 860°C for 30 min, followed by glass removal and drive-in at 1050°C for 60 min; surface passivation was achieved by the growth of a thin, invisible (<20 nm) passivating oxide at 900°C for 20 min in O_2 and 10 min in Ar followed by an anneal in forming gas at 400°C. These four wafers, labelled A, B, C and D, have essentially the same emitter region and surface passivation conditions (two were subsequently de-passivated to investigate the sensitivity of violet response to the surface passivation quality). Their sheet resistance was 42–54 Ω/sq, which happens to be similar to that of industrial solar cells, although the dopant profile is quite different, with a lower surface concentration and a deeper junction. Additional high resistivity FZ wafers with a 5 Ω/sq more heavily doped and deeper emitter were also prepared by increasing the drive-in temperature to 1100°C. An industrial phosphorus diffusion

Table 2
Optical absorption fraction, f_{abs} calculated for a 300 μm thick bare silicon wafer at different light wavelengths. The value of f_{abs} corresponding to the AM1.5G white light has been referred to a total maximum short-circuit current of 43.13 mA/cm^2

Illumination	White AM1.5G	$\lambda = 410$ nm	$\lambda = 700$ nm	$\lambda = 1000$ nm	$\lambda = 1050$ nm
Absorption fraction, f_{abs}	0.597	0.533	0.662	0.612	0.329
Absorption depth, $1/\alpha$ (μm)	~10	0.15	5.26	156	613

was performed in a conveyor belt furnace on similar p-type FZ silicon wafers. The resulting emitter had a sheet resistance of 70 Ω/sq, which, despite being slightly higher than the targeted value, is still representative of commercial solar cell technology based on screen printing metallisation. The rear surface of these wafers received a light, well passivated phosphorus diffusion in the laboratory.

A contactless inductively coupled photoconductance apparatus[2] was used to measure wafer lifetime with the quasi-steady-state technique [1]. Monochromatic illumination at 410 and 1000 nm was obtained by interposing colour filters between the xenon flash and the wafers. The width of the band passed by the filters was 10 nm. Even after filtering, high (greater than 10 suns) light intensities could be achieved. This makes the use of bias light unnecessary. Heating is still minimal, due to the short duration of the light pulse. The light intensity varies by a factor of 150 within the 12 ms pulse, and this automatically scans the dependence of the photoconductance with injection level. A correct mathematical analysis of the quasi-steady-state conditions [11] allows an accurate determination of the lifetime even in cases where it is sufficiently high as to make the simple steady-state assumption unacceptable, such as the millisecond-lifetime samples discussed below. A spectrally calibrated detector (a SunPower high efficiency concentrator silicon solar cell) was used to determine the incident photon flux, N_{ph}. To circumvent the need for reflectivity and transmission measurements of the test samples we have used very thin (<20 nm) oxides, which ensures a reflectivity practically identical to that of bare silicon, and modelled with PC1D the optical absorption fraction, f_{abs}. Table 2 gives the values of f_{abs} calculated at different wavelengths for the case of 300-μm-thick silicon wafers with no antireflection coating.

Relevant experimental results are summarised in Table 3. The first two wafers labelled A and B are particularly relevant because they have a common solar cell base resistivity, 1 Ω cm. The only difference between these two wafers is in the front surface passivation, with the thin SiO_2 layer still present on wafer A and having been stripped from wafer B. The two base regions and rear surfaces are identical, and, as implied by the value of effective lifetime measured for sample A, they are known to have a minimum bulk carrier lifetime of $\tau_{bulk} \geqslant 130\,\mu s$, equivalent to a diffusion length $L_{bulk} \geqslant 590\,\mu m$ (using $D_n = 27\,cm^2/s$), and a maximum effective surface recombination velocity $S_{rear} \leqslant W/(2\tau_{eff}) = 115\,cm/s$. It is important to note that the

[2] Sinton Consulting, 1132 Green Circle, Boulder, CO 80305, USA.

Table 3
Wavelength-dependent measurements of the steady-state effective lifetime of float zone silicon wafers with different phosphorus diffusions, surface passivation conditions and base resistivities, and corresponding internal emitter collection efficiencies at 410 nm

Sample	ρ_{bulk} (Ω cm)	Emitter R_{sheet} (Ω/sq)	Surface passivation	τ_{eff} (μs) $\lambda = 410$ nm	τ_{eff} (μs) $\lambda = 1000$ nm	$\eta_{c-emitter}$ (410)
A	1	50	Yes both	130	130	1
B	1	52	Front no, rear yes	10.5	35	0.3
I	1	70 (industrial)	Front no, rear yes	20	27	0.74
C	50	42	No both	215	715	0.3
D	50	42	Yes both	2020	2000	1
#5	50	5	Yes both	470	1600	0.29
#5	50	5	No both	195	1200	0.16

removal of the surface passivation does not only affect the UV emitter collection efficiency, but also the overall recombination in the device, that is, the lifetime measured at $\lambda = 1000$ nm. The change of $\tau_{eff}(\lambda = 1000\,nm)$ is very strong for these samples, from 130 to 35 μs. The latter value implies that the effective surface recombination velocity of the de-passivated front floating emitter is $S_{front} \leqslant 742$ cm/s for sample B. Such analysis, based on IR measurements, ignores the inner properties of emitter regions and considers them as mere boundary conditions at the end surfaces of the base region. The additional UV measurements provide a deeper insight into carrier recombination and transport within the emitter. The ratio between the UV and IR spectral lifetime values is, as expressed by Eq. (17), approximately identical to the emitter collection efficiency for violet light. Our measurements indicate that $\eta_{emitter}(\lambda = 410\,nm) \approx 1$ for wafer A, with an experimental uncertainty of about 10%, and $\eta_{emitter}(\lambda = 410\,nm) \approx 0.3$ for wafer B. This shows the expected detrimental effect of a non-passivated surface.

The experiment also included a pair of identical wafers of 50 Ω cm resistivity, labelled C and D. After verifying that both wafers had initially the same effective lifetime, the passivating oxide was etched from both surfaces of wafer C. The removal of the front and rear oxides reduced the effective lifetime from 2000 to 715 μs, as measured with IR light. With the emitter surface passivated by a thin silicon dioxide layer (sample D), the effective lifetime is nearly the same for the two wavelengths, which indicates $\eta_{emitter}(\lambda = 410\,nm) \approx 1$. After etching the passivating oxide (sample C), the effective lifetime dropped markedly for the case of violet light, and $\tau_{eff}(\lambda = 410\,nm)/\tau_{eff}(\lambda = 1000\,nm) \approx 0.3$, in excellent agreement with the simultaneously processed 1 Ω cm wafers.

A third high resistivity, phosphorus diffused wafer given in Table 3 is sample #5. This wafer has a very heavily doped and deep emitter with $R_{sheet} = 5\,\Omega$/sq. In this case the experimental results indicate a drop of $\eta_{emitter}(\lambda = 410\,nm)$ from 0.29 to 0.16 upon etching of the passivating oxide. The low collection efficiency of 0.29 even with a passivating oxide is due to prevalent recombination in the bulk of the emitter. This shows that the method is not only sensitive to surface passivation conditions but also to the bulk properties of the emitter.

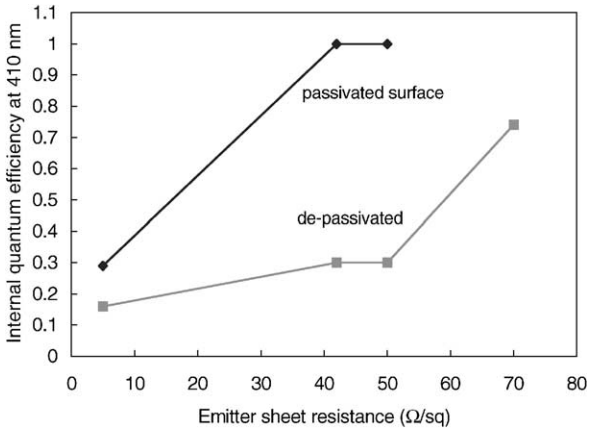

Fig. 5. Internal quantum efficiency at 410 nm obtained from spectral photoconductance measurements for a variety of wafers having different phosphorus diffusions. The 70 Ω/sq diffusion was fabricated in a commercial belt furnace. See Table 2 for details.

The emitter collection efficiencies at 410 nm measured for the different single crystal FZ silicon wafers with and without a passivating oxide are summarised in Fig. 5. With the exception of the 70 Ω/sq emitter, which was diffused in a conveyor belt furnace and is relatively shallow (approximately 0.3 μm), these wafers have a thick emitter region (1–2 μm), especially the 5 Ω/sq diffusion. This makes them very sensitive to the wavelength of the illumination used to measure the photoconductance. The ability of the latter to discriminate emitter quantum efficiencies in a broad range between 16% and 100% is clearly demonstrated by these experimental results. In light of the discussion of appropriate choices of long-wavelength reference, it would have been better to have used 700–800 nm rather than 1000 nm for the long-wavelength reference. PC1D simulations indicate that for the cases in Fig. 4, the errors due to this poor choice of 1000 nm light are negligible for the passivated case, less than $\pm 15\%$ for the unpassivated wafers at 5–50 Ω/sq, and an estimated 25% for the 70 Ω/sq case.

Since the effective lifetime usually varies with the excess carrier density, we have measured it for the two wavelengths over a broad range of light intensities and taken the two values of lifetime at the same carrier density, near the maximum of the curves. The complete injection-dependent lifetime measurements for wafers C and D using either UV or IR monochromatic illumination are shown in Fig. 6. From the highest injection part of the data in Fig. 6 it is possible to extract the saturation current density of the emitter region, J_{oe} [2]. The result is different for the different wavelengths. For example, the data for wafer C with violet light give $J_{oe} = 3500\,\mathrm{fA/cm^2}$, much higher than the value obtained with IR light, $750\,\mathrm{fA/cm^2}$. We can thus make the important observation that the determination of J_{oe} from quasi-steady-state illumination can be affected by the wavelength of the light. Mid to long wavelengths should, therefore, be used to measure the saturation current density J_{oe}

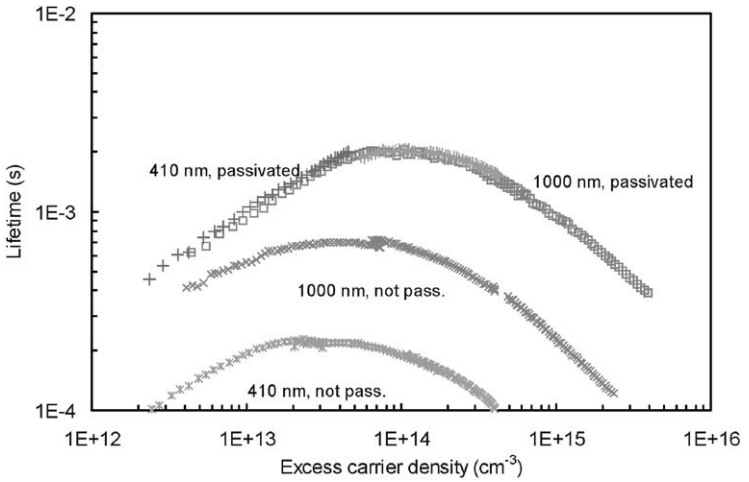

Fig. 6. Effective lifetime as a function of carrier injection level for two high resistivity silicon wafers measured with UV (410 nm) and IR (1000 nm) light. One wafer has passivated surfaces, while the other wafer is not passivated. See details of wafers C and D in Table 2.

when it is very high, as in unpassivated emitters, and violet–blue light (<700 nm) should be filtered out if white light is used and a high precision is desired.

6. Conclusions

We have shown that the steady-state photoconductance measured under monochromatic illumination can be a useful characterisation tool for solar cell emitters. The method described in this paper indicates that in addition to the well-established determination of the wafer recombination properties that results from a long-wavelength measurement, detailed emitter quantum-efficiency information is available by performing a second measurement with UV light. The method is appropriate for routine monitoring of the emitter region of solar cells in a simple, contactless manner. For technologies resulting in emitters with high quantum efficiencies and long wafer effective lifetimes (high voltage), the method mimics the spectral response of short-circuit current at all wavelengths. For wafers with poor emitter quantum efficiencies or low effective lifetimes, the window of applicability is restricted in wavelength. In most cases a choice of 400–450 and 700–800 nm for the UV and IR wavelengths, respectively, should be appropriate to evaluate the emitter quantum-collection efficiency.

Acknowledgements

The Australian Research Council has provided support for this work. Thanks to C. Samundsett of ANU and BPSolar Australia for sample processing.

References

[1] R.A. Sinton, A. Cuevas, Appl. Phys. Lett. 69 (1996) 2510.
[2] A. Cuevas, M. Stocks, D. Macdonald, R. Sinton, Applications of the quasi-steady-state photoconductance technique, Second World Conference on Photovoltaic Solar Energy Conversion, Vienna, European Commission, 1998, p. 1236.
[3] R. Sinton, Proceedings of the Nineth Workshop on Crystalline Silicon Solar Cell Materials and Processes, Breckenridge, Colorado, National Renewable Energies Laboratory, 1999, p. 67.
[4] J. Schmidt, A. Cuevas, J. Appl. Phys. 86 (1999) 3175.
[5] A. Cuevas, R.A. Sinton, Progress in Photovoltaics 5 (1997) 79.
[6] H. Nagel, B. Lenkeit, R.A. Sinton, A. Metz, R. Hezel, Relationship between effective carrier lifetimes in silicon determined under steady-state and transient illumination, Proceedings of the 16th European Photovoltaic Solar Energy Conversion, Glasgow, European Commission, 2000, p. 93.
[7] M. Bail, R. Brendel, Separation of bulk and surface recombination by steady state photoconductance measurements, Proceedings of the 16th European Photovoltaic Solar Energy Conversion, Glasgow, European Commission, 2000, p. 98.
[8] A. Cuevas, Sol. Energy Mater. Sol. Cells 57 (1999) 277.
[9] P. Basore, D. Clugston, PC1D version 4 for Windows: from analysis to design, Proceedings of the 25th Photovoltaic Specialists Conference, Washington, IEEE, New York, 1996, p. 377.
[10] P.A. Basore, Extended analysis of internal quantum efficiency, Proceedings of the 23rd Photovoltaic Specialists Conference, Louisville, IEEE, New York, 1993, p. 147.
[11] H. Nagel, C. Berge, A.G. Aberle, J. Appl. Phys. 86 (1999) 6218.